Int J Earth Sci (Geol Rundsch) (2017) 106:341–353
DOI 10.1007/s00531-016-1322-3

ORIGINAL PAPER

The use of HVSR measurements for investigating buried tectonic structures: the Mirandola anticline, Northern Italy, as a case study

G. Tarabusi[1,2] · **R. Caputo**[2,3]

Received: 14 September 2015 / Accepted: 14 March 2016 / Published online: 9 April 2016

Abstract The Mirandola anticline represents a buried fault-propagation fold which has been growing during Quaternary due to the seismogenic activity of a blind segment belonging to the broader Ferrara Arc. The last reactivation occurred during the May 2012 Emilia sequence. In correspondence with this structure, the thickness of the marine and continental deposits of the Po Plain foredeep is particularly reduced. In order to better define the shallow geometry of this tectonic structure, and hence its recent activity, we investigated in a depth range which is intermediate between the surficial morphological observations and seismic profiles information. In particular, we carried out numerous passive seismic measurements (single-station microtremor) for obtaining the horizontal-to-vertical spectral ratio. The results of a combined analysis of the peak frequency and its amplitude nicely fit the available geological information, suggesting that this low-cost geophysical technique could be successfully applied in other sectors of wide morphologically flat alluvial plains to investigate blind and completely buried potential seismogenic structures.

Keywords Seismic hazard · Seismotectonics · Single-station microtremor · HVSR · Blind anticline · Po Plain

✉ G. Tarabusi
gabriele.tarabusi@ingv.it

[1] Istituto Nazionale di Geofisica e Vulcanologia, Via di Vigna Murata 605, 00143 Rome, Italy

[2] Department of Physics and Earth Sciences, Ferrara University, Via Saragat 1, 44122 Ferrara, Italy

[3] Research and Teaching Center for Earthquake Geology, Tyrnavos, Greece

Introduction

In May 2012, two moderate ($M_L = 5.9$ and 5.8 or $M_w = 6.1$ and 5.9; e.g. Pondrelli et al. 2012) earthquakes, associated with a noticeable aftershock sequence (e.g. Saraò and Peruzza 2012; Scognamiglio et al. 2012), affected the eastern sector of the Po Plain, Italy. The causative faults are two segments of the Ferrara Arc thrust system representing the most frontal portion of the buried Northern Apennines fold-and-thrust belt (e.g. Vannoli et al. 2015; Fig. 1a). In particular, the two major structures which were reactivated have a left-stepping largely overlapping geometry. Both seismogenic sources were associated with blind, mainly dip-slip reverse, faulting (e.g. Scognamiglio et al. 2012; Pondrelli et al. 2012), while the uppermost tip segment of the sliding planes has been estimated to reach a minimum depth of 3–4 km (Bignami et al. 2012). As a consequence of the fault geometry and kinematics, the rock volume above the co-seismic rupture tip was characterized by a typical fault-propagation folding process that eventually caused the bending of the topographic surface and the consequent uplift of the broader epicentral area (Fig. 1b; Bignami et al. 2012; Salvi et al. 2012; Pezzo et al. 2013; Caputo et al. 2015).

However during the long interseismic periods, the high sedimentation rate characterizing the Po Plain tends to compensate the seismically induced topographic variations. The repeating of similar 'areal morphogenic earthquakes' (Caputo 2005) during Late Pleistocene and Holocene locally caused cumulative effects in the coeval stratigraphic succession. Although such stratigraphic lateral variations are relatively evident in the deeper geology (Pieri and Groppi 1981; Boccaletti et al. 2004), they are morphologically subtle in the otherwise

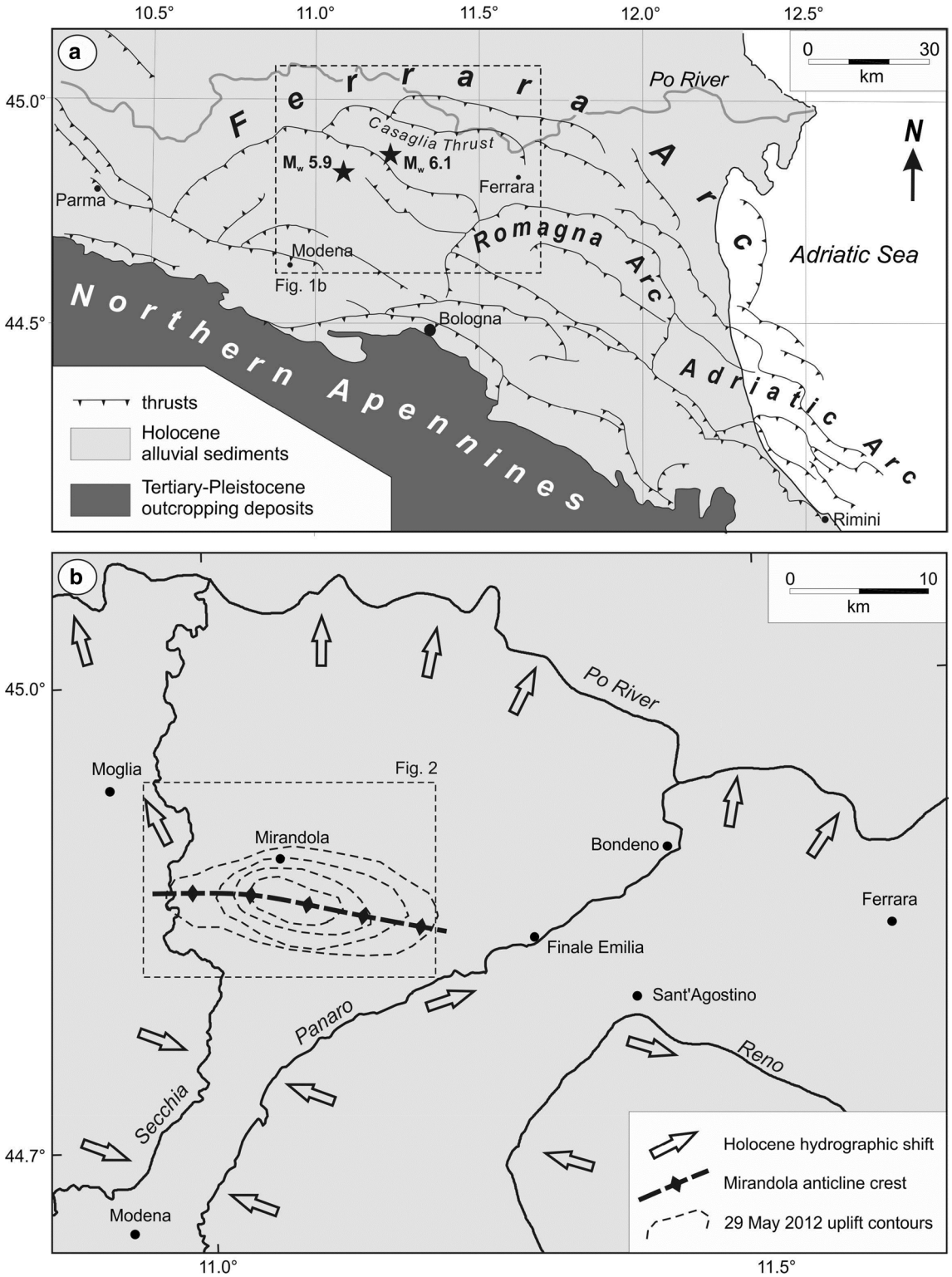

Fig. 1 **a** Tectonic sketch map of the buried Northern Apennines fold-and-thrust belt. *Stars* represent the epicentres of 20 May (M_w 6.1) and 29 May (M_w 5.9) 2012 earthquakes. Modified from Bigi et al. (1992). **b** The major hydrographic changes and path migrations (*arrows*) occurred in the Holocene caused by the persisting activity of blind tectonic structures belonging to the Northern Apennines. The trace of the Mirandola anticline and the coseismic uplift contours of the May 29 events (Pezzo et al. 2013) are also shown

flat topography of the alluvial plain and they could be emphasized only by a careful inspection of the hydrographic network, which indeed highlights the occurrence of several drainage anomalies (e.g. Burrato et al. 2003, 2012; Fig. 1b). Such hydrographic anomalies were considered key features for documenting the recent tectonic activity of the underlying faults (Basili et al. 2008; DISS WG 2015) whose instrumental or even historical seismic record is relatively poor due to the long recurrence intervals on these structures.

In the present paper, we focus on the shallow subsoil, say the first 100–200 m, representing an intermediate-depth investigation target between the deep geological elements and the surface features. The former could be only observed based on very expensive seismic reflection profiles generally carried out for hydrocarbon purposes; however, these geophysical surveys are not always available, but above all the details for the uppermost stratigraphic levels are commonly not sufficient to document the most recent tectonic activity of blind thrusts. Indeed, due to the deeper target of such explorations, the analysis of the uppermost sediments, which could potentially record a recent seismogenic activity, are often deliberately neglected since the preliminary planning phases of the geophysical survey. On the other hand, the results of detailed topographic, hydrographic and morphological analyses could be masked or even obliterated by the effects of anthropogenic manipulations and the fluvial dynamics occurring during the long interseismic periods, which are commonly in the order of thousands of years.

For the above reasons, in the present research we investigated the natural amplification occurring within the subsoil due to the presence of impedance contrasts. In particular, we focused on the area of Mirandola and its surroundings for two main reasons. Firstly, because this is a small-/medium-size industrial district and hence of particular economic and social interest for Italy. Secondly, because the urban area is in correspondence with a growing fault-propagation anticline whose top is at <100 m depth and where both the causative thrust and the associated fold are completely buried by the Middle–Upper Pleistocene to Holocene continental deposits (e.g. Martelli and Molinari 2008; Bonini et al. 2014). The differential vertical movements induced by this blind tectonic structure and especially the positive ones (i.e. uplift in correspondence with the fold hinge) are not able to keep pace with the regional scale subsidence and the high sedimentation rates of the Po Plain. Therefore, we wanted to test the systematic application of a low-cost geophysical technique in order to gather useful information on the local, relatively shallow, stratigraphy as well as of its seismic behaviour. This in turn could help in constraining some crucial seismotectonic parameter and hence improving seismic hazard analyses.

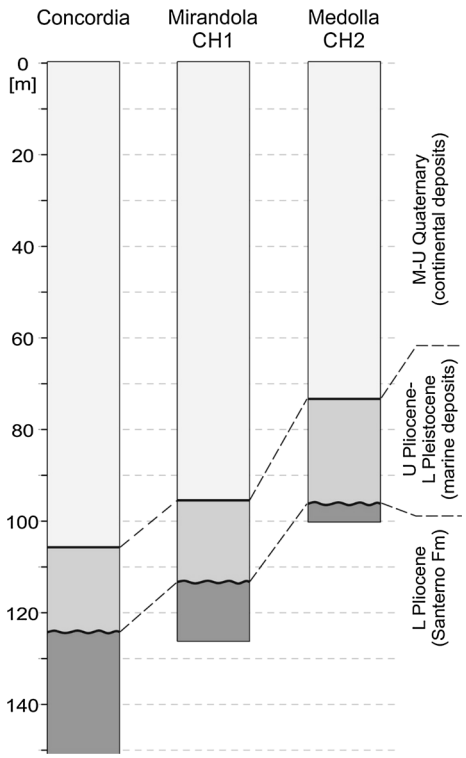

Fig. 2 Simplified lithological and stratigraphic logs of the Concordia, Mirandola and Medolla boreholes. In the latter two, the cross-hole surveys (CH1 and CH2, respectively) used for the calibration of the HVSR measurements have been performed. See Fig. 3 for locations

The occasion of starting this scientific project was the preparation of a seismic microzonation map for the Municipality of Mirandola, Emilia-Romagna (Northern Italy). This investigation was commissioned in winter 2011–2012, and the report complete of maps was released few months before the seismic sequence that affected the broader area (Tarabusi 2012). It is noteworthy that the areas characterized by the strongest damage in May 2012 (likely induced by local amplification effects) were perfectly identified and already clearly depicted in these preliminary results.

For the specific aims of the present paper, numerous passive seismic measurements (single-station microtremor analyses) were additionally performed in order to improve and especially enlarge the database originally collected for the microzonation study and thus extend the investigated area to cover the whole Mirandola anticline. Accordingly, the major targets of this note are, firstly, to investigate an area much wider than the original microzonation study and

Table 1 Geographic coordinates (latitude and longitude) of the HVSR measurements and the corresponding natural frequency, f_0, and peak value, A

Label	Lat.	Lon.	f_0[a]	A
H001	44.8894	11.0702	0.91	2.2
H002	44.8821	11.1963	0.78	2.1
H003	44.8943	11.1793	0.75	2.3
H004	44.8842	11.0714	0.84	2.5
H005	44.8854	11.0782	0.88	2.4
H006	44.8905	11.0819	0.89	2.2
H007	44.8940	11.0686	0.88	2.1
H008	44.8884	11.0634	0.78	2.2
H009	44.8694	11.0610	0.88	3.9
H010	44.8779	11.0552	0.88	3.8
H011	44.8875	11.0527	0.72	2.4
H012	44.8907	11.0341	0.88	2.7
H013	44.8856	11.0433	0.88	3
H014	44.8826	11.0639	0.81	2.7
H015	44.8790	11.0631	0.94	3.3
H016	44.8609	11.0595	1.03	5.7
H017	44.8701	11.0482	1.03	4.4
H018	44.8958	11.0878	0.78	2.2
H019	44.8854	11.0670	0.84	2.4
H020	44.8619	11.0623	1.09	4.6
H021	44.8623	11.0564	1.06	5.8
H022	44.8977	11.0708	0.88	2.2
H024	44.8749	11.1277	0.94	2.2
H025	44.8590	11.0441	0.94	3.2
H026	44.8737	11.0094	1.22	3.7
H027	44.8761	11.0194	1.03	3.6
H028	44.8809	11.0484	0.84	3.5
H029	44.9185	11.1025	0.81	2
H030	44.9217	11.0911	0.9	1.9
H031	44.9012	11.0688	0.94	2.1
H032	44.8924	11.0752	0.91	2.1
H033	44.8908	11.0597	0.75	2.2
H034	44.8804	11.0554	0.84	3.2
H035	44.8732	11.0454	1.09	3.4
H036	44.8530	11.0374	0.87	2.1
H037	44.8669	11.0560	1.09	4.2
H038	44.8779	11.0751	0.91	2.5
H039	44.8696	11.0651	1	4.1
H040	44.8677	11.0641	1.19	4.3
H041	44.8656	11.0693	1.06	4.4
H042	44.8893	11.1014	0.93	1.8
H043	44.8811	11.0263	1.13	3.6
H044	44.8849	11.0285	1.06	3.2
H045	44.8636	11.0194	0.88	2.2
H046	44.9168	11.0654	0.93	2.3
H047	44.8766	11.0906	0.63	2.2
H048	44.8722	11.0807	0.91	2.7
H049	44.8684	11.0760	0.91	4.1
H050	44.8748	11.0683	0.94	3
H051	44.8593	11.0563	1.03	3.5
H052	44.8552	11.0511	0.94	2.7
H053	44.8654	11.0265	1.06	2.8
H054	44.8700	11.0281	1.16	3.2
H055	44.8729	11.0001	1.41	3.1
H056	44.8670	11.0098	1.03	2.4
H057	44.8586	11.0279	0.88	1.9
H058	44.8507	11.0459	0.72	1.8
H059	44.8815	11.0694	0.84	2.4
H062	44.8887	11.0573	0.81	2.1
H064	44.8772	11.1332	0.91	2
H065	44.8734	11.1015	0.72	2.8
H066	44.8657	11.0959	0.91	3.8
H067	44.8463	11.0888	0.88	2.9
H068	44.8329	11.0770	0.92	2
H069	44.8573	11.0927	1.03	5.3
H070	44.8443	11.0701	0.75	2.9
H071	44.8446	11.0560	0.72	2
H072	44.8739	11.0345	1.06	4.1
H073	44.8589	11.0882	1.06	4.7
H074	44.8775	11.0629	0.88	3.6
H075	44.8370	11.1589	0.78	2.4
H076	44.8507	11.1733	0.72	2.1
H077	44.8737	11.1861	0.78	2.4
H078	44.8824	11.1614	0.75	2.1
H079	44.8650	11.1522	0.84	2.2
H080	44.8359	11.1379	0.78	2.5
H081	44.8241	11.1000	0.89	1.9
H082	44.8438	11.1069	0.81	3
H083	44.8548	11.1107	1.06	4.1
H084	44.8701	11.1200	0.75	2.7
H085	44.8664	11.0818	0.91	5.3
H086	44.8553	11.0748	1.16	3.9
H087	44.8362	11.0637	0.81	2.4
H089	44.8268	11.1622	0.88	1.9
H090	44.8436	11.1697	0.72	2.6
H091	44.8624	11.1779	0.81	2.5
H092	44.8727	11.1547	0.81	2.5
H093	44.8563	11.1505	0.88	2.8
H094	44.8453	11.1453	0.84	4.2
H095	44.8238	11.1323	0.84	2.2
H096	44.8331	11.1056	0.75	2
H097	44.8624	11.1139	0.91	4.4
H098	44.8606	11.0772	1.03	5.4
H099	44.8507	11.0712	0.94	4.1
H100	44.9113	10.9943	0.88	2.2
H101	44.8834	10.9884	1.19	4.4

Table 1 continued

Label	Lat.	Lon.	f_0[a]	A
H102	44.8422	10.9564	0.94	1.9
H103	44.8778	10.9653	2	4.1
H104	44.8706	10.9751	1.38	5.1
H105	44.8785	10.9910	1.44	3.9
H106	44.9223	11.0320	0.75	2
H107	44.8931	11.0111	0.84	2.4
H108	44.8684	11.0028	1.13	3.4
H109	44.8321	11.0316	0.88	2.1
H110	44.9224	10.9955	0.81	2.3
H111	44.8982	10.9902	0.84	2.1
H112	44.8584	10.9670	0.84	2.3
H113	44.8768	10.9839	1.53	4.7
H114	44.8932	10.9985	0.84	2.2
H115	44.8844	11.0070	1.06	3.6
H116	44.8596	11.0000	0.91	1.9
H117	44.8915	11.1109	0.81	2.1
H118	44.9002	11.0763	0.91	2.4
H119	44.8944	11.0591	0.81	2.3
H120	44.8901	11.0956	0.94	2.4
H121	44.8986	11.0816	0.88	2.1
H122	44.9022	11.0594	0.94	2.3
H123	44.8537	11.0691	1	4.4
H124	44.8807	11.0769	0.84	2.3
H125	44.8478	11.0620	0.94	2.1
H126	44.9061	10.9703	0.84	2.3
H127	44.9013	10.9618	0.88	2.3
H128	44.8933	10.9729	0.88	3
H129	44.8877	10.9636	1.13	3.1
H130	44.8560	10.9552	0.94	1.9
H131	44.8688	10.9556	1.13	4.1
H132	44.8822	10.9570	1.69	4.1
H133	44.8625	10.9850	0.94	2.8
H134	44.8586	11.1254	0.94	3.1
H135	44.8500	11.1347	0.94	2.9
H136	44.8635	11.0609	1.13	5

[a] Uncertainty on f_0 is commonly around 0.05 with few exception up to 0.15 in case of particularly broad peaks

corresponding to the broader Mirandola anticline region and, secondly, to define the best procedure and a general protocol for systematically applying the methodology to similar geological and tectonic settings of the Po Plain and worldwide.

Methodology

The passive seismic measurements have been taken using a digital tromograph (Tromino$^{(R)}$) that records the background noise in order to obtain the natural resonance frequencies within the underground. All measurements have been taken in free field conditions far from buildings in order to avoid their effects and to solely investigate the subsoil stratigraphy. We followed the three general reliability conditions proposed in the SESAME user guidelines (Koller et al. 2004; Bard et al. 2005). Then natural resonance frequency has been also directly correlated with local seismic amplification which is commonly considered as the principal source of damage in case of earthquake shaking (e.g. Mucciarelli et al. 2001; Gallipoli et al. 2004). The background noise, also referred to as microtremor, is present everywhere at the Earth's surface and could be associated also with both atmospheric phenomena and anthropogenic activities. It is generally characterized by very small oscillations with spectral components poorly attenuated in space and measurable with passive recording techniques. All elastic waves during their path from the source to a site suffer some attenuation which is basically geometric, due to the increasing dimensions of the wave front, and anelastic, due to the real not perfectly elastic behaviour of all rocks. In both cases, the amount of attenuation is a function of frequency; indeed, assuming a constant velocity for all frequencies, the shorter the wavelength (i.e. the higher the frequency), the greater the number of cycles and hence of the attenuation occurred. Accordingly, stratigraphic layering governs the distribution of the mechanical properties (e.g. Castellaro et al. 2005). Such information is included in the recorded microtremors together with random noise, and it can be extracted by means of several methods like the one proposed by Nakamura (1989; horizontal-to-vertical spectral ratio, HVSR). This technique is nowadays largely used in order to determine the local seismic amplification and to estimate the principal resonance frequencies characterizing the shallow subsoil, say from tens to few hundreds of meters. Both outcomes are crucial for engineering antiseismic planning.

The H/V method assumes the microtremors as mainly consisting of Rayleigh waves, both vertical and horizontal components, which are amplified as a consequence of site effects induced by the presence of stratigraphic discontinuities within the subsoil. Based on a Fourier transform, it is thus possible to reconstruct, in the frequency domain, the spectral distribution of both horizontal and vertical records (measured in the time domain) and hence calculate the HVSR. The occurrence of a peak in the HVSR curve documents the presence of a mechanical discontinuity along the vertical of the measured site.

The field work was carried out with three different instruments, and several tests have been performed by repeating the measurements at a same site at different times for checking repeatability of results. Sampling was at 128 Hz with recording times between 30 and 12 min

according to the SESAME criteria (Koller et al. 2004; Bard et al. 2005) for a reliable H/V curve. The Grilla software (Micromed 2006, 2008) was used for elaborating the records within the frequency interval 0–64 Hz, considering time windows of 20 s and a smoothing technique based on a 10 % wide triangular window.

Natural frequencies and amplitudes

Within a strongly subsiding foredeep basin, like the Po Plain since Middle Pleistocene, in correspondence with the structural culminations of the fault-propagation anticlines, the thickness of the continental Quaternary deposits is generally reduced. Moreover, these deposits generally consist of condensed sedimentary successions or even temporal *hiatuses*, and in the investigated region, they directly overlay the Pliocene marine units (Pieri and Groppi 1981; Boccaletti et al. 2004; Martelli and Molinari 2008). As a consequence, a high impedance contrast occurs due to the abrupt increase in both seismic waves velocity and material density (Fig. 2). Accordingly, these mechanical conditions are favourable to be detected on the basis of HVSR analyses (Amorosi et al. 2008).

In particular, when the lithological changes are sharp and stratigraphically reduced to (less than) few meters, a high and marked amplification peak is expected to form in the HVSR curve. As commonly accepted in the literature, the frequency of the amplification peak is at a first approximation proportional to the shear wave velocity of the overlying sedimentary body and to the inverse of the discontinuity depth according to the formula (the so-called resonance equation)

$$f_0 = \frac{v_s}{4 \cdot h} \quad (1)$$

In some sectors of the buried anticline, a relatively thin layer of Upper Pliocene–Lower Pleistocene marine deposits (even just 20–30 m) could be interposed between the overlying 'condensed' continental sedimentary succession

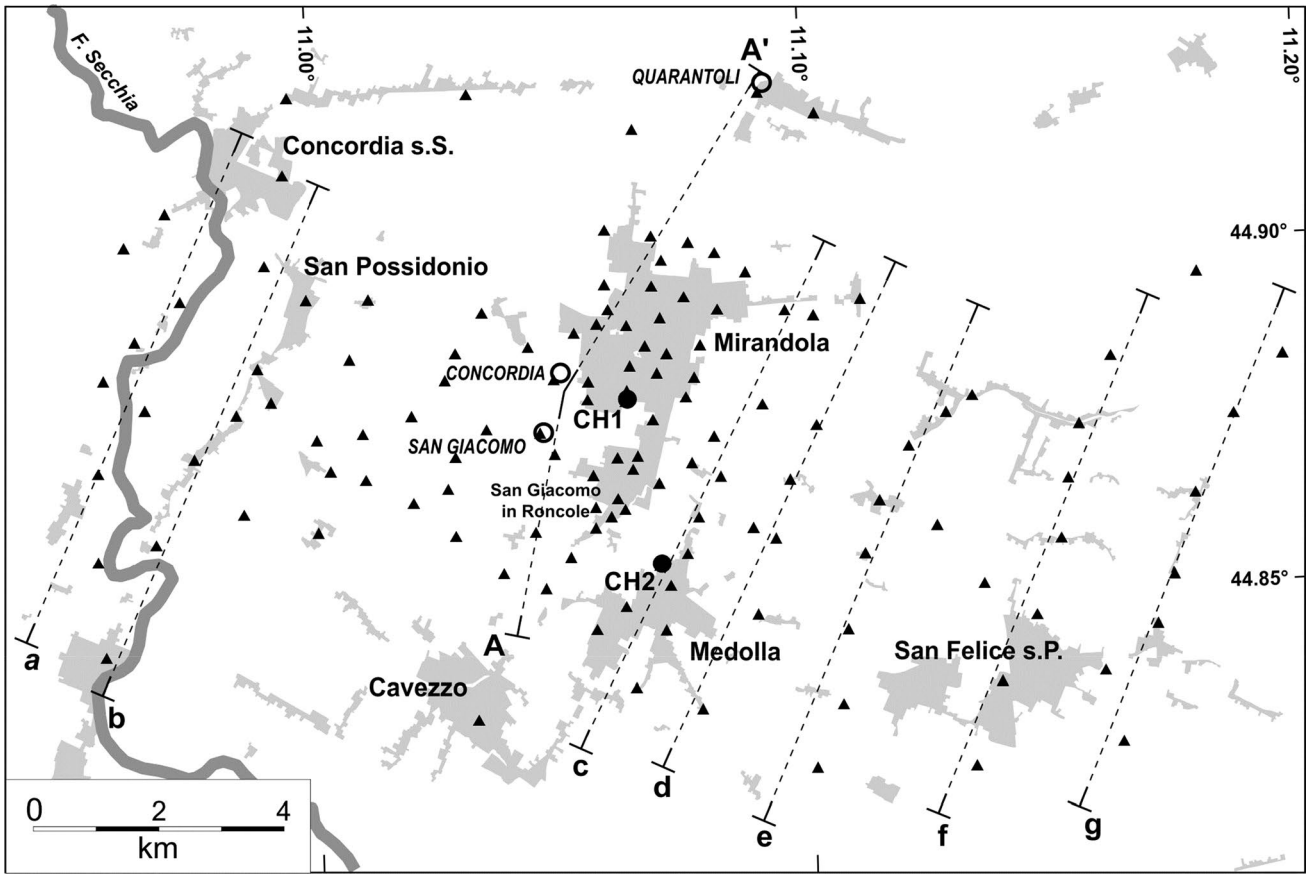

Fig. 3 Map of the investigated area showing the distribution of the HVSR measurements (*triangles*). *A–A′* indicate the trace of the seismic reflection profile represented in Fig. 7, while *a–g* indicate the traces of the profiles shown in Fig. 9. *Full circles* indicate the Mirandola (CH1) and Medolla (CH2) boreholes used for measuring the seismic waves velocity profiles shown in Fig. 7, while empty circles indicate the deep boreholes used to interpret section *A–A′* (corresponding names are in *italics*)

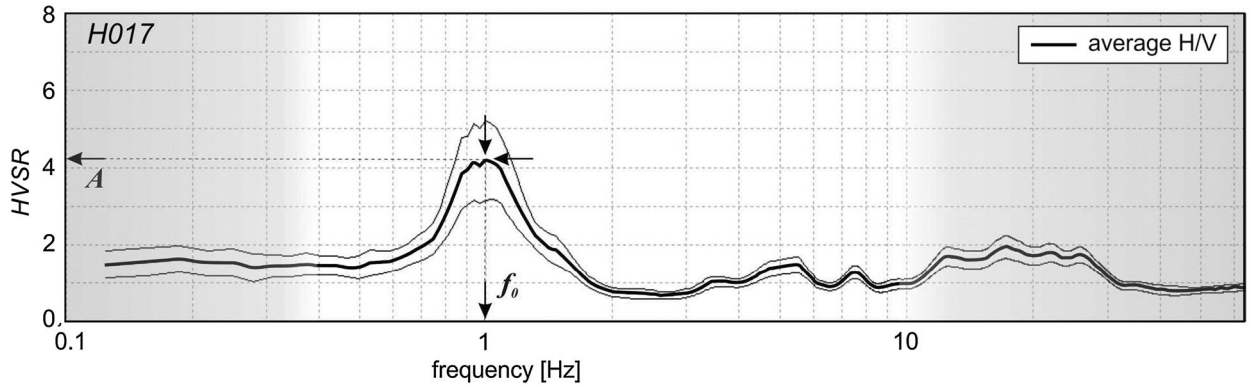

Fig. 4 Example of HVSR curve (site *H017*) showing the average H/V ratio as a function of the frequency as well as the corresponding standard deviations (*thin lines*). The *arrows* emphasize the values considered for the purpose of this paper in terms of the natural frequency, f_0, and maximum amplitude of the ratio (A). The shaded areas indicate the disregarded parts of the graph (see text for discussion)

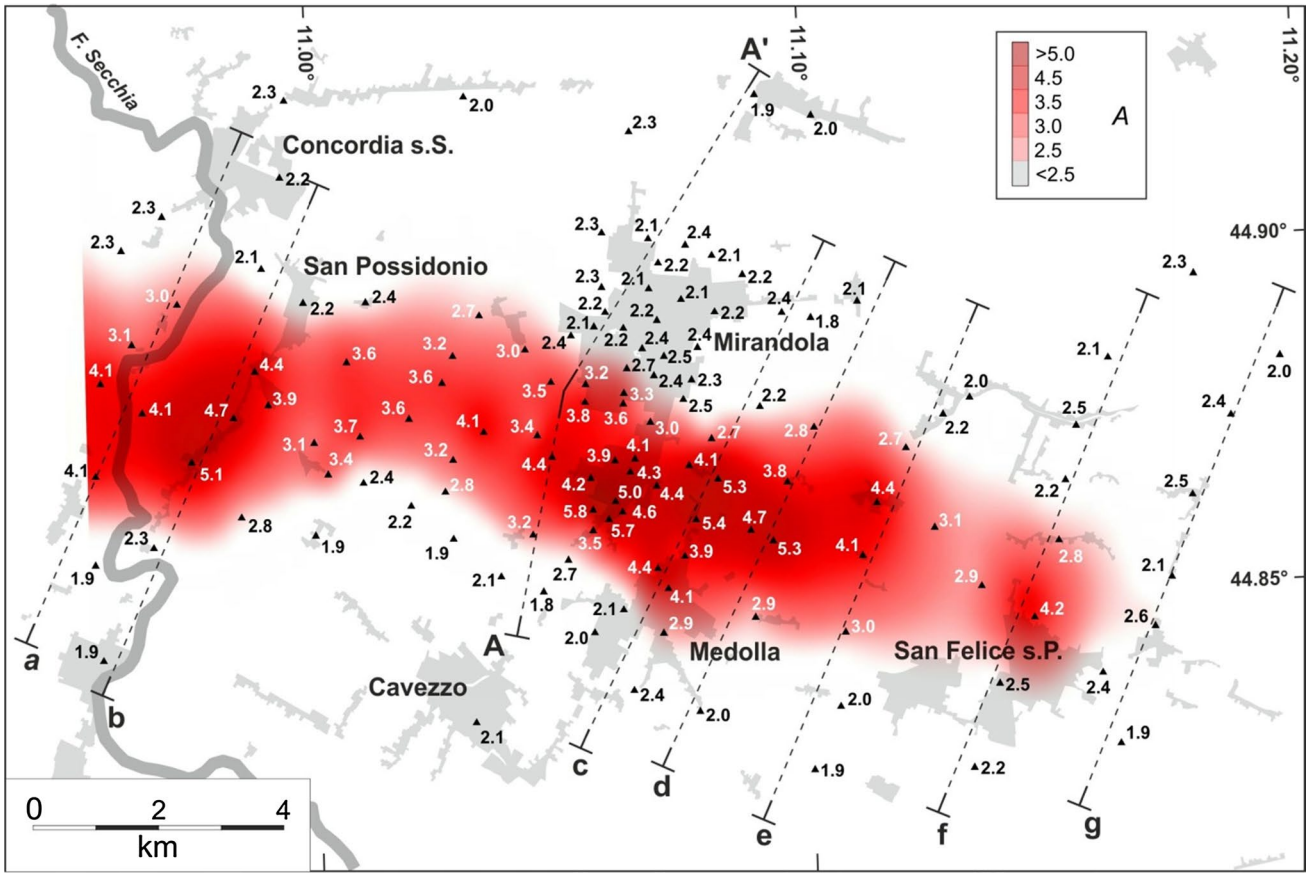

Fig. 5 Distribution of the HVSR peak amplitude, A, obtained within the investigated area. The *darker the colour*, the higher the value and hence the strongest the impedance contrast. *Triangles* indicate the measured sites. Corresponding numerical values are also reported in Table 1

and the underlying lithological units (Fig. 2). In this geological setting, the impedance contrast is somehow distributed or possibly split between more than one surface. In this case, the HVSR analysis shows two (or more) very close peaks or a relatively wide one (Oliveto et al. 2004; Castellaro et al. 2005).

In principle, the higher the peak, the greater the impedance contrast between the two layers, while the narrower

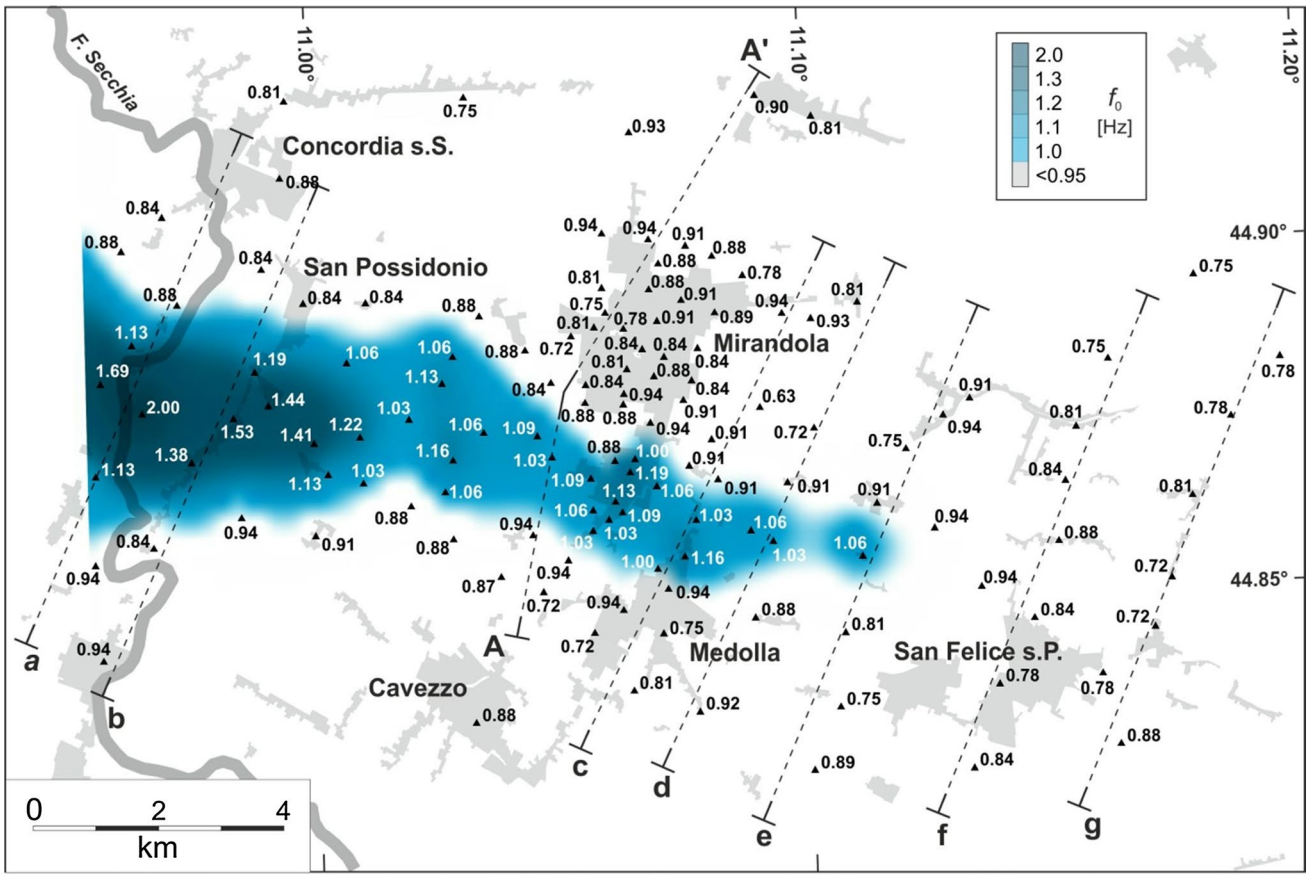

Fig. 6 Distribution of the HVSR natural frequency, f_0, obtained within the investigated area. The *darker the colour*, the higher the value and hence the shallower the surface characterized by the impedance contrast. *Triangles* indicate the measured sites. Corresponding numerical values are also reported in Table 1

the peak (i.e. characterized by a very small range of frequencies), the sharper is the lithological variation in the stratigraphic column.

Data distribution

During the geophysical campaigns, a total number of about 150 free field measurements have been taken. About 10 % of them were discarded according to the SESAME criteria and based on the single-component Fourier spectra, or because they were affected by anthropogenic disturbances. Accordingly, only 131 measurements have been further considered and subsequently analysed for the purpose of this paper (Table 1). They are distributed all over the investigated area (Fig. 3), though with a variable density in order to better highlight the geometry of the Mirandola anticline, which represents the structure-related stratigraphy investigated in this paper. As mentioned earlier, for each site the amplitude of the peak value of the HVSR curve, A, and the corresponding frequency, f_0 (commonly referred to as *natural frequency*), have been considered (an example is shown in Fig. 4). In this regard, it should be noted that only the peaks between 0.2–0.4 and ~10 Hz have been analysed. Indeed, peaks at lower frequencies could be possibly influenced by the meteorological conditions (Koller et al. 2004), while peaks at $f_0 > 10$ Hz are associated with very shallow stratigraphic reflectors of no interest for the purpose of this paper.

The distribution of both parameters has been further elaborated by creating a colour-shaded map using the Kriging interpolation method included in Golden Software Surfer(R). The results of the geophysical campaign and the gridding clearly document the presence of areas characterized by resonance phenomena, locally very important ones, and allow to map their distribution. In particular, Fig. 5 evidences the occurrence of a narrow zone (2.5–3.5 km wide), trending ESE–WNW and characterized by A values of the HVSR curves (Fig. 4) >2.5. Local maxima occur, from west to east, along the central sector.

A similar pattern is also observed in Fig. 6, where the natural frequency f_0 has been interpolated with the same procedure described above. In this case, the selected discriminant value

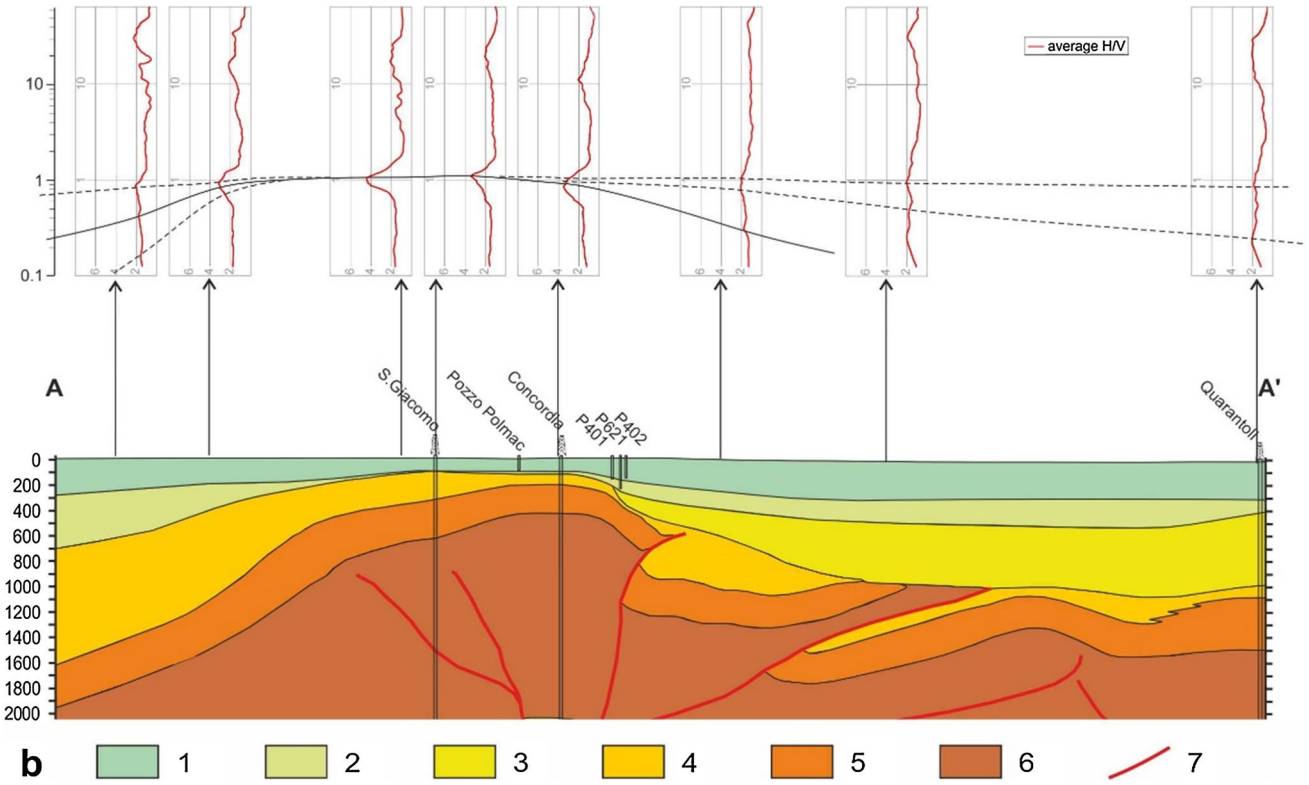

Fig. 7 **a** HVSR curves obtained from sites investigated within a distance of 200 m from a profile crossing the Mirandola anticline (*A*–*A*′ in Fig. 3). The major peaks in the different graphs have been tentatively correlated along the transect suggesting the possible lateral continuity of the surfaces characterized by some impedance contrast. See for comparison the parallel geological section (**b**) obtained from a seismic reflection profile and boreholes data (modified from Martelli and Molinari 2008). Legend: *1* Middle–Upper Quaternary continental deposits; *2* Upper Pliocene–Lower Pleistocene marine deposits; *3* Middle Pliocene; *4* Santerno Formation (Lower Pliocene); *5* Porto Garibaldi Formation (Lower Pliocene); *6* Colombacci Formation (Upper Messinian); *7* major thrusts

is ca. 1 Hz and the gridding emphasizes an elongated ESE–WNW-trending area characterized by natural frequencies up to 2.0 Hz. Assuming as a first approximation laterally uniform (or smoothly variable) seismic waves velocities within the uppermost sedimentary units, say the first 100–150 m, the mapped distribution of the natural frequencies is certainly due to a strongly variable depth of the surface producing the resonance (i.e. characterized by an impedance contrast).

The areas emphasized in Figs. 5 and 6 basically coincide and are both characterized by marked gradients north and south and progressive fading ESE-wards. Position and dimensions of the overlapping area as well as the corresponding values of the two mapped parameters are due to laterally changing impedance contrast associated with the variable stratigraphic succession developed during Pliocene–Quaternary on top of the Mirandola anticline.

Interface depth

A geological cross section based on seismic reflection profiles (Martelli and Molinari 2008) and realized for investigating possible geothermal reservoirs in the area of Mirandola is represented for reference in Fig. 7b. On top of the profile are also plotted the HVSR curves obtained from sites measured within a distance of ca. 200 m from the trace of the geological section (*A*–*A*′ in Fig. 3). Accordingly, we tentatively correlated laterally the major peaks and few secondary ones in order to obtain a pseudo-2D section representing the principal surfaces characterized by impedance contrast. As it could be clearly observed, there is a good agreement between the reconstructed subsoil geometry of the Pliocene and Quaternary sedimentary bodies and the position (i.e. frequency) and shape of the peaks in the different HVSR curves (Fig. 7a). In particular, in correspondence with the top of the Mirandola anticline, the HVSR curves show a marked peak, locally as high as 5.8, progressively decreasing in amplitude *A* both northwards and southwards, that is to say moving towards the two contiguous synclines. From a mechanical and hence seismological point of view, these HVSR variations (Fig. 7a) could be due to a laterally variable impedance contrast particularly related to an impedance increase in the sedimentary body below the interface in correspondence with the anticline. This could be a consequence of (1)

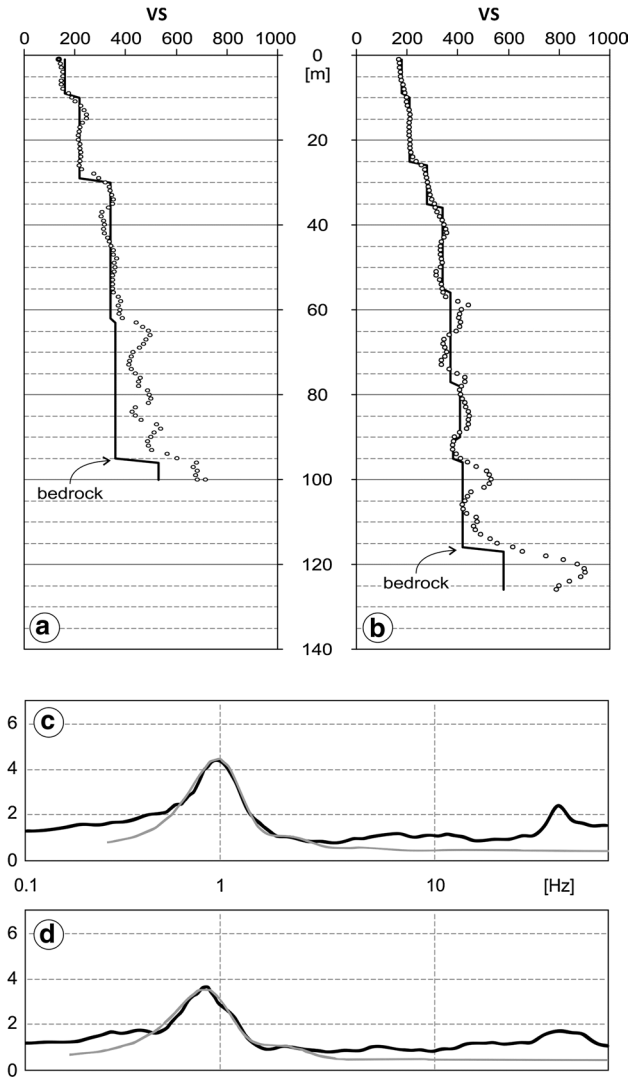

Fig. 8 1D velocity profiles obtained at Medolla (**a**) and Mirandola (**b**) (see Fig. 3 for location) with the cross-hole technique (*dots*). **c**, **d** The HVSR curves measured at the head site of the two boreholes (*black curves*) and the modelled ones (*grey curves*) obtained using the simplified velocity profile shown in (**a**, **b**) as a stepping *black curve*

differential compaction, (2) the direct contact with older (i.e. more compacted and denser) layers following the partial erosion of the upper part of the underlying succession and/or (3) a condensed overlying sedimentary series. Following the same approach, we also attempted to correlate other secondary peaks (Fig. 7a), which emphasize the pinch-out geometry of the sedimentary bodies infilling the synclines both north and south of the Mirandola anticline.

Discussion

It is worth to note that the overall picture of the buried Mirandola anticline has been obtained in this paper based only on the large number of single-station measurements that allowed to laterally correlate the peak frequency and amplitude of the HVSR curves and especially to give a stratigraphic meaning to the interfaces corresponding to the observed peaks (Figs. 5, 6).

In order to further constrain and validate the subsoil model here proposed, we also carried out HVSR measurements in correspondence with two boreholes cored by Regione Emilia-Romagna down to a depth of 101 and 127 m, respectively (see Fig. 3 for location). Accordingly, at these two sites, the detailed stratigraphic succession has been reconstructed showing the occurrence of the lower Pliocene Top, the so-called seismic pseudo-bedrock interface of the area (i.e. $v_s \geq 600$ m/s). at ca. 96 and 113 m, respectively (Luca Martelli, pers. comm.). Moreover, at both sites a second borehole was drilled to perform a cross-hole investigation for measuring the velocity distribution at depth (Fig. 8a, b). Based on a simplified inversion approach (Castellaro and Mulargia 2009), we succeeded to reproduce our measured HVSR curves and particularly the major and meaningful peaks down to the bedrock interface separating the marine Early Quaternary–Late Pliocene from Lower Pliocene deposits (Fig. 8c, d). The slight velocity misfit with increasing depth is possibly due to the progressive loss of verticality and hence of parallelism between the two boreholes used for the cross-hole measurements that could have introduced a velocity error in the deeper part of the borehole measurement (e.g. Butler and Curro 1981).

Following the resonance Eq. (1), a good estimate of the shear-waves velocity of the deposits overlying the lithological discontinuity could allow to constrain its depth. The estimated values of the v_{s30} and especially of the v_{sH} vary from 200 to 210 m/s and from 305 to 315 m/s, respectively, at the two measured sites of Medolla and Mirandola (Fig. 8a, b). Accordingly, the inferred depth of the recognized discontinuity emphasized by the natural frequency distribution (Fig. 6) ranges between 75 and 90 m, on the crest of the Mirandola anticline (e.g. near San Giacomo in Roncole; Fig. 3), to more than 150 m both north and south along the two flanks of the fold and towards the eastern pericline (the investigated area does not cover the western termination of the buried tectonic structure).

Although in laterally heterogeneous sedimentary successions a much larger number of boreholes would be necessary to establish a reliable frequency–thickness relationships (e.g. Ibs von Seht and Wohlenberg 1999; Gosar and Lenart 2010), our investigated area is characterized by a smoothly variable stratigraphy, and hence, we consider the calibration performed at the two boreholes of Regione Emilia-Romagna as sufficiently constrained for the purpose of this paper.

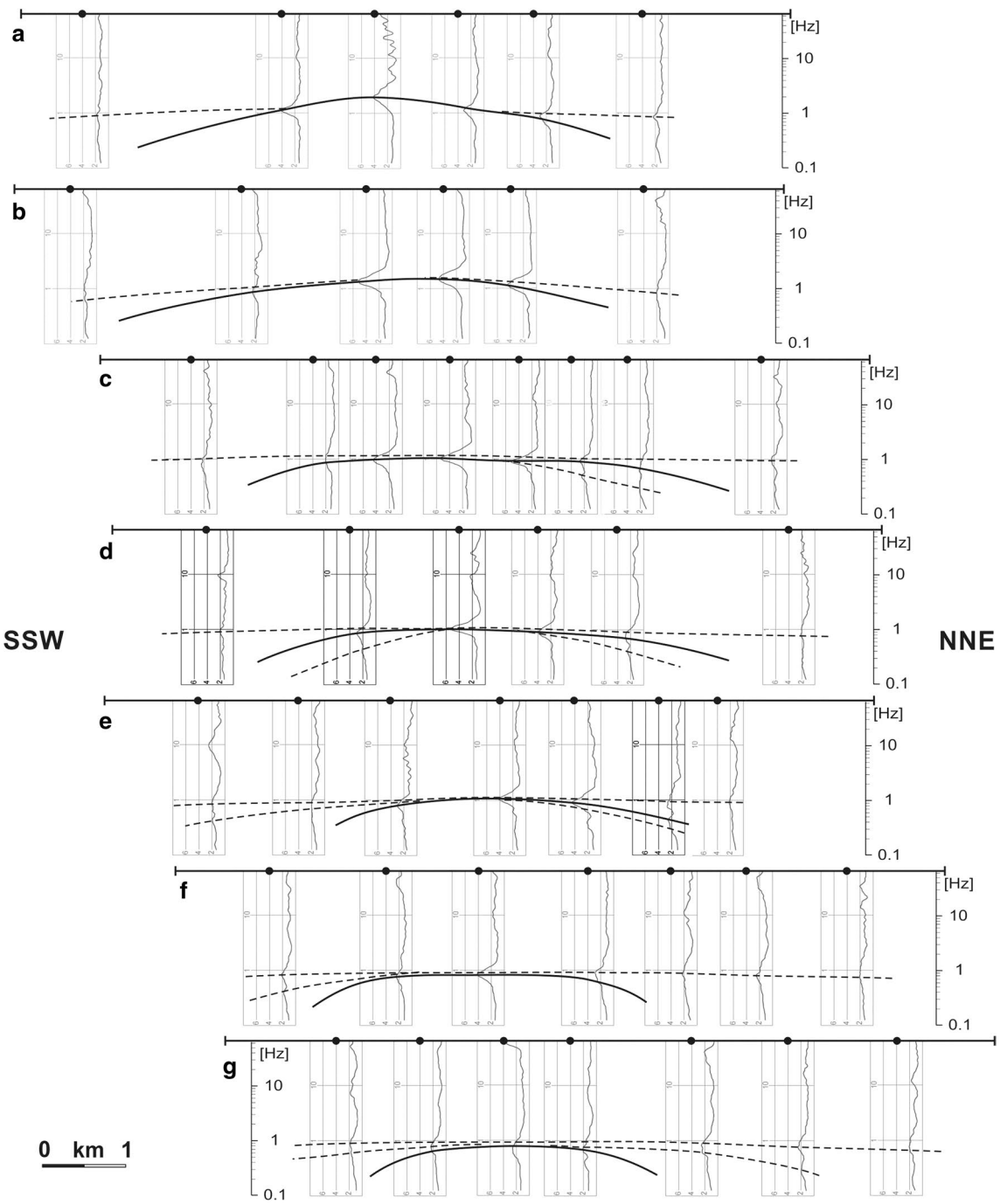

Fig. 9 HVSR curves obtained from sites investigated within a distance of 200 m from the traces *a–g* (see Fig. 3 for location) crossing the Mirandola anticline. Following the same approach discussed in the text and shown in Fig. 7, the major peaks have been tentatively correlated to form pseudo-2D sections

According to the calibrated mean velocity profiles and following the same approach previously described and used for laterally correlating 1D HVSR measurements (Fig. 7a), we elaborated several transects oriented NNE–SSW that are running across the buried anticline (traces *a* to *g* in Fig. 3). The results of this approach and the tentative correlations among the different HVSR peaks are shown in Fig. 9, where it is possible to observe a substantially uniform pattern marked by some major surfaces (i.e. characterized by impedance contrast) converging both north and south towards the top of the anticline. This geometry is emphasized by

the more pronounced and relatively higher frequency peaks, which commonly correspond to the shallowest depth of the so-called seismic pseudo-bedrock (i.e. $v_s \geq 600$ m/s).

Concluding remarks

Seismic amplification is influenced by the stiffness of the soil, and especially by the impedance contrast among shallow seismic units. Accordingly, maps of natural frequency are of utmost importance because they allow to recognize areas characterized by a high impedance contrast where a greater amplification in ground motion is expected to occur in case of seismic shaking. Indeed, if the amplified frequency at a site is close to that of a standing building, a resonance effect may occur, and therefore, the risk of the building to suffer structural damage greatly increases (e.g. Mucciarelli et al. 2001; Castellaro et al. 2014). In this regard, amplification maps are crucial for urban planners in defining the height of buildings (viz. the number of floors) characterized by a resonance coincident with the natural one and enabling engineers to improve the antiseismic behaviour of new constructions or to retrofit old ones. Seismic amplification is in fact considered the first cause of damage and collapse during an earthquake (e.g. Mucciarelli et al. 2001; Gallipoli et al. 2004).

The major results of the present research consist in the reconstruction of the natural amplification distribution associated with, and caused by, the presence of impedance contrast in the subsoil. In particular, this information has been obtained either in terms of frequency and amplitude of the HVSR (Figs. 5, 6). This paper also shows how the systematic application of the HVSR method, a low-cost non-invasive geophysical technique, generating a relatively dense grid of measurements over a wide area and strictly following as a standard the well-tested SESAME criteria, could allow to laterally correlate specific amplification peaks and hence to interpolate with confidence the same impedance contrast surface. According to the instrumentation used and the stratigraphic setting of the investigated area, such a surface that represents the real target of the whole procedure could be up to 150–200 m deep. The capacity to model it in some detail could enable to map large-scale deformations, which are too subtle to be reconstructed on the basis of morphological analyses (due to the lack of cumulative effects) and generally too shallow to be taken into account during seismic reflection surveys devoted to hydrocarbon exploration.

Finally, the application of the above procedure to the Mirandola case study allowed to emphasize the persisting and recent growth of a major fault-propagation anticline, where both the causative thrust and the associated fold are completely buried by the Middle–Upper Pleistocene to Holocene continental deposits (e.g. Martelli and Molinari 2008; Bonini et al. 2014). In this regard, the obtained results clearly and independently document the presence of a folded surface in the shallow Mirandola subsoil; the crest is oriented ESE–WNW with a culmination towards the west and a periclinal setting eastwards in perfect agreement with the deeper tectonic structure reconstructed on the basis of seismic reflection profiles. The results of this methodological approach are quite encouraging and could be easily applied to other morphologically flat regions affected by blind faulting and folding.

Acknowledgments We are grateful to Luca Martelli and Silvia Castellaro for their valuable and helpful suggestions. The pre-events microzonation study was financially supported by the Municipality of Mirandola and the Italian Dipartimento di Protezione Civile in the frame of an agreement with the regional administrations (OPCM 3907/2010, DGR 1051/2011).

References

Amorosi A, Castellaro S, Mulargia F (2008) Single-station passive seismic stratigraphy: an inexpensive tool for quick subsurface investigations. GeoActa 7:29–39

Bard P-Y, Acerra C, Alguacil G, Anastasiadis A, Atakan K, Azzara R, Basili R, Bertrand E, Bettig B, Blarel F, Bonnefoy-Claudet S, Bordoni P, Borges A, Bøttger-Sørensen M, Bourjot L, Cara F, Caserta A, Chatelain J-L, Cornou C, Cotton F, Cultrera G, Daminelli R, Dimitriu P, Dunand F, Duval A-M, Fäh D, Fojtikova L, de Franco R, di Giulio G, Grandison M, Guéguen P, Guillier B, Haghshenas E, Havskov J, Jongmans D, Kind F, Kirsch J, Koehler A, Koller M, Kristek J, Kristekova M, Lacave C, La Rocca M, Marcellini A, Maresca R, Margaris B, Moczo P, Moreno B, Morrone A, Ohrnberger M, Ojeda JA, Oprsal I, Pagani M, Panou A, Paz C, Querendez E, Rao S, Rey J, Richter G, Rippberger J, Roquette P, Roten D, Rovelli A, Saccoroti G, Savvaidis A, Scherbaum F, Schisselé E, Spühler-Lanz E, Tento A, Teves-Costa P, Theodulidis N, Tvedt E, Utheim T, Vassiliadès J-F, Vidal S, Viegas G, Vollmer D, Wathelet M, Woessner J, Wolff K, Zacharapoulos S (2005) Guidelines for the implementation of the H/V spectral ratio technique on ambient vibrations measurements, processing and interpretation. Deliverable D23.12 of the SESAME project, April 2005. http://www.SESAME-FP5.obs.ujf-grenoble.fr

Basili R, Valensise G, Vannoli P, Burrato P, Fracassi U, Mariano S, Tiberti MM, Boschi E (2008) The Database of Individual Seismogenic Sources (DISS), version 3: summarizing 20 years of research on Italy's earthquake geology. Tectonophysics 453(1–4):20–43. doi:10.1016/j.tecto.2007.04.014

Bigi G, Bonardini G, Catalano R, Cosentino D, Lentini F, Parlotto M, Sartori R, Scandone P, Turco E (1992) Structural model of Italy, 1:500,000. Consiglio Nazionale delle Ricerche, Rome

Bignami C, Burrato P, Cannelli V, Chini M, Falcucci E, Ferretti A, Gori S, Kyriakopoulos C, Melini D, Moro M, Novali F, Saroli M, Stramondo S, Valensise G, Vannoli P (2012) Coseismic deformation pattern of the Emilia 2012 seismic sequence imaged by Radarsat-1 interferometry. Ann Geophys 55(4):788–795. doi:10.4401/ag-6157

Boccaletti M, Bonini M, Corti G, Gasperini P, Martelli L, Piccardi L, Tanini C, Vannucci G (2004) Seismotectonic

Map of the Emilia-Romagna Region, 1:250000. Regione Emilia-Romagna—CNR

Bonini L, Toscani G, Seno S (2014) Three-dimensional segmentation and different rupture behavior during the 2012 Emilia seismic sequence (Northern Italy). Tectonophysics 630:33–42. doi:10.1016/j.tecto.2014.05.006

Burrato P, Ciucci F, Valensise G (2003) An inventory of river anomalies in the Po Plain, Northern Italy: evidence for active blind thrust faulting. Ann Geophys 46(5):865–882

Burrato P, Vannoli P, Fracassi U, Basili R, Valensise G (2012) Is blind faulting truly invisible? Tectonic-controlled drainage evolution in the epicentral area of the May 2012, Emilia-Romagna earthquake sequence (Northern Italy). Ann Geophys 55(4):525–531. doi:10.4401/ag-6182

Butler DK, Curro JR (1981) Crosshole seismic testing; procedures and pitfalls. Geophysics 46(1):23–29. doi:10.1190/1.1441134

Caputo R (2005) Ground effects of large morphogenic earthquakes. J Geodyn 40(2–3):113–118

Caputo R, Pellegrinelli A, Bignami C, Bondesan A, Mantovani A, Stramondo S, Russo P (2015) High-precision levelling, DInSAR and geomorphological effects in the Emilia 2012 epicentral area. Geomorphology 235:106–117. doi:10.1016/j.geomorph.2015.02.002

Castellaro S, Mulargia F (2009) Vs30 estimates using constrained H/V measurements. Bull Seismol Soc Am 99:761–773. doi:10.1785/0120080179

Castellaro S, Mulargia F, Bianconi L (2005) Passive seismic stratigraphy: a new efficient, fast and economic technique. J Geotech Environ Geol 3:51–77

Castellaro S, Padròn LA, Mulargia F (2014) The different response of apparently identical structures: a far-field lesson from the Mirandola 20th May 2012 earthquake. Bull Earthq Eng 12(5):2481–2493. doi:10.1007/s10518-013-9505-9

DISS WORKING GROUP (2015) Database of Individual Seismogenic Sources (DISS), Version 3.2.0: a compilation of potential sources for earthquakes larger than M 5.5 in Italy and surrounding areas. http://diss.rm.ingv.it/diss/, ©INGV 2015—Istituto Nazionale di Geofisica e Vulcanologia—All rights reserved. doi:10.6092/INGV.IT-DISS3.2.0

Gallipoli MR, Mucciarelli M, Gallicchio S, Tropeano M, Lizza C (2004) Horizontal to vertical spectral ratio (HVSR) measurements in the area damaged by the 2002 Molise, Italy, earthquake. Earthq Spect 20(S1):S81–S93. doi:10.1193/1.1766306

Gosar A, Lenart A (2010) Mapping the thickness of sediments in the Ljubljana Moor basin (Slovenia) using microtremors. Bull Earthq Eng 8:501–518. doi:10.1007/s10518-009-9115-8

Ibs-von SM, Wohlenberg J (1999) Microtremor measurements used to map thickness of soft sediments. Bull Seismiol Soc Am 89(1):250–259

Koller M, Chatelain J-L, Guillier B, Duval A-M, Atakan K, Bard P-Y, SESAME Team (2004) Practical user guidelines and software for the implementation of the H/V ratio technique: measuring conditions, processing method and results interpretation. In: 13th World conference earthquake engineering, Vancouver, August 2004, proceedings, paper # 3132

Martelli L, Molinari FC (2008) Studio geologico finalizzato alla ricerca di potenziali serbatoi geotermici nel sottosuolo del comune di Mirandola, Regione Emilia Romagna. Internal Report, Servizio Geologico, Sismico e dei Suoli, Bologna, p 26

Micromed (2006) Grilla ver. 2.2, spectral and HVSR analysis—user's manual. Micromed, Treviso, p 47

Micromed (2008) An introduction to the phase velocity spectra module in Grilla. Micromed, Treviso, p 16

Mucciarelli M, Contri P, Mochavesi G, Calvano G, Gallipoli MR (2001) An empirical method to assess the seismic vulnerability of existing buildings using the HVSR technique. Pure Appl Geophys 158:2635–2647

Nakamura Y (1989) A method for dynamic characteristics estimation of subsurface using microtremor on the ground surface. Quart Rep Railw Tech Res Inst RTRI 30:25–33

Oliveto AN, Mucciarelli M, Caputo R (2004) HVSR prospections in multi-layered environments: an example from the Tyrnavos Basin (Greece). J Seismol 8:395–406

Pezzo G, Merryman Boncori JP, Tolomei C, Salvi S, Atzori S, Antonioli A, Trasatti E, Novali F, Serpelloni E, Candela L, Giuliani R (2013) Coseismic deformation and source modeling of the may 2012 Emilia (Northern Italy) earthquakes. Seismol Res Lett 84(4):645–655. doi:10.1785/0220120171

Pieri M, Groppi G (1981) Subsurface geological structure of the Po Plain, Italy. Consiglio Nazionale delle Ricerche, Progetto finalizzato Geodinamica, sottoprogetto Modello Strutturale, pubbl. No. 414, Roma

Pondrelli S, Salimbeni S, Perfetti P, Danecek P (2012) Quick regional centroid moment tensor solutions for the Emilia 2012 (northern Italy) seismic sequence. Ann Geophys 55(4):615–621. doi:10.4401/ag-6146

Salvi S, Tolomei C, Merryman Boncori JP, Pezzo G, Atzori S, Antonioli A, Trasatti E, Giuliani R, Zoffoli S, Coletta A (2012) Activation of the SIGRIS monitoring system for ground deformation mapping during the Emilia 2012 seismic sequence, using COSMO-SkyMed InSAR data. Ann Geophys 55(4):796–802. doi:10.4401/ag-6181

Saraò A, Peruzza L (2012) Fault-plane solutions from moment-tensor inversion and preliminary Coulomb stress analysis for the Emilia Plain. Ann Geophys 55(4):647–654. doi:10.4401/ag-6134

Scognamiglio L, Margheriti L, Mele FM, Tinti E, Bono A, De Gori P, Lauciani V, Lucente FP, Mandiello AG, Marcocci C, Mazza S, Pintore S, Quintiliani M (2012) The 2012 Pianura Padana Emiliana seimic sequence: locations, moment tensors and magnitudes. Ann Geophys 55(4):549–556. doi:10.4401/ag-6159

Tarabusi G (2012) Microzonazione sismica del comune di Mirandola. Quadro conoscitivo del PSC di Mirandola. http://www.comune.mirandola.mo.it/la-citta-e-il-territorio/piano-strutturale-comunale-psc. Studio di Geologia Tarabusi, QB_C_REL1, 26 Jan 2012, Bologna, p 57

Vannoli P, Burrato P, Valensise G (2015) The seismotectonics of the Po Plain (Northern Italy): tectonic diversity in a blind faulting domain. Pure Appl Geophys 172:1105–1142. doi:10.1007/s00024-014-0873-0